Personal project report
Simulation of a particle detector

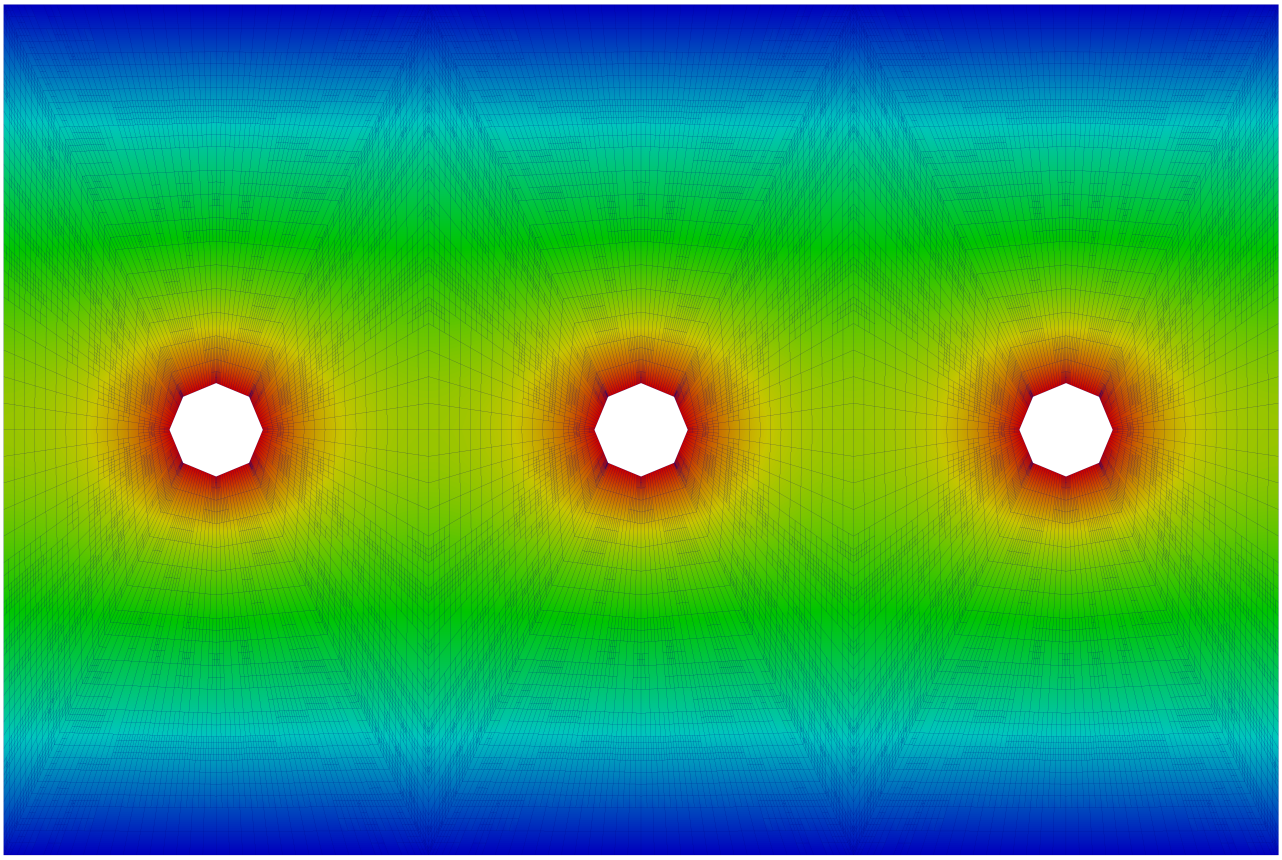

Arnaud Schils
Simon Lardinois

2015-2016

Table of contents

Introduction and objectives

Nowadays, the huge amount of computing power offered by modern computer systems allows to solve complex scientific problems numerically. The art of solving physics problems using computers is referred as *computational physics*. This modern field is multidisciplinary: it brings together applied mathematics, computer science and physics. It offers a third way to do physics that supplements theory and experiment.

In this work, these numerical techniques are applied to the field of particle detector physics. In order to design the best detectors, physicists have to know the measured signal resulting from the passage of a particle in the detector. Unfortunately, due to the complex geometries of these detectors and the various physical phenomena to handle, this signal is not easy to compute analytically.

The objective of this work is to develop a software to compute the current measured by a particle detector due to the passage of a particle. In its final version, the software will generate the detector induced current for three-dimensional geometries. To efficiently achieve this goal, the software may be improved to take advantage of the processing power offered by clusters and GPUs [1]. Furthermore, a maximum of the relevant physical effects happening in particle detectors will be implemented. Additional types of medias (Ar, H_2,...), particles and energy deposit distributions will be handled. Finally, a simulation of the electronic will be implemented. This work is a first step to reach this objective. The software developed in the context of this work, *Pdetect*, has been used to study silicon and gas particle detectors. The source code is available on *Github* at the following address: `https://github.com/aschils/pdetect`.

Overview of the contributions

The primary contribution of this thesis is the development of a C++ numerical software performing the following tasks.

Firstly, it computes the potential and the electric field at each point of a particle detector solving the Poisson equation

$$\nabla^2 V = -\frac{\rho}{\epsilon}$$

for non-trivial two-dimensions geometries. Currently, the charges distribution is supposed to be $\rho = 0$ inside the detector and the solved equation is rather the Laplace equation:

$$\nabla^2 V = 0$$

Three types of 2D detector geometries are supported. The Laplace equation is solved using the *finite element method* with an adaptive grid refinement strategy. The software supports multithreading and therefore uses all available CPUs to quickly solve this equation.

Secondly, the software computes the current resulting from the passage of a particle in the detector using the *Shockley–Ramo theorem* and the solution of the computed electric field. Every possible

[1] Graphics Processing Unit.

particle trajectories in the detector are supported. Effects such as the *mobility* difference between charge carriers, *saturation* phenomena and the *Townsend Avalanche* are handled.

This software has been developed following the object-oriented programming paradigm and with the *model-view-controller* software engineering pattern in mind. Thanks to the quality of the software architecture further extensions such as 3D geometries, additional physical effects or detector types and the support of distributed computations on clusters are possible without the burden of reimplementing an entire new software.

The secondary contribution of this thesis is the use of this software to study the gas and silicon detectors. Finally, the results provided by the software have been compared with the results of *Weightfield* [16], a software performing similar computations.

Examples of other softwares able to perform the same tasks are *Garfield* [8] and *Comsol* [2]. The first one simulates two- and three-dimensional gas detectors. *Garfield* heavily relies on external programs. It accepts maps computed by finite element programs such as *Ansys*, *Maxwell*, *Tosca*, *QuickField* and *FEMLAB*. It relies on *Magboltz* to compute electron properties in gas and *Heed* to simulate ionization of the media molecules. The second one is a more general commercial software able to solve various physics and engineering problems using finite element methods.

Organization of the work

This work is organized in six Sections. The remainder of this manuscript is structured as follows.

- Section 1 introduces the finite element method and the C++ finite element library `deal.ii`. Then, *Weightfield*, a software simulating particle detectors, is presented.
- Section 2 is a resume of the detector physics concepts that must be known to understand the problem solved by the software developed in the context of this thesis.
- Section 3 presents the features of the software and the actions it performs in chronological order.
- Section 4 presents the results obtained with our software for different set of parameters which models various detectors.
- Appendix A presents further comparisons between the numerical and analytical solutions of the potential.
- Appendix B explains the software architecture and the role played by the most important classes.
- Appendix C answers questions related to the academic activity such as what was the most difficult part of the project, how the project was conducted and the distribution of tasks between the authors.

1 Background and related work

This section is composed of three parts. Firstly, the finite element method is briefly explained. Then *deal.ii*, a C++ library implementing the finite element method is introduced. Finally, *Weightfield*, another software performing particle detector simulation, is presented.

1.1 Finite element method

The finite element method is a numerical technique for finding approximate solutions to boundary value problems for partial differential equations [6]. The finite element method subdivides a large problem into smaller, simpler, parts, called finite elements. The simple equations that model these finite elements are then assembled into a larger system of equations that models the entire problem. It then uses variational methods from the calculus of variations to approximate a solution by minimizing an associated error function.

A finite element method is characterized by:

1. a *variational formulation* such as the *Galerkin methods* [7]. These methods convert a differential equation to a discrete problem.

   The *Galerkin methods* models the domain of interest by a mesh and considers the restriction of the searched function on each element of the mesh. These restrictions are then approached by polynomials on each element.

2. a *discretization strategy* i.e. procedures to generate the finite element meshes, select the basis function on reference elements and map the reference elements on the mesh elements.

   A non-exhaustive list of discretization strategies contains the *h-version*, *p-version*, *hp-version*, *x-FEM* and *isogeometric analysis* strategies. Each discretization strategy has pros and cons.

3. one or more *solution algorithms*. There are two types of solution algorithms: direct and iterative solvers [14]. These solvers solve the linear system

   $$Ax = b$$

   where A is large, sparse and ill-conditioned [2].

   The direct solvers always work for any invertible matrix and are faster for smaller problems. However, they consume more memory and are slower for larger problems. The iterative solvers have a good spatial complexity ($\mathcal{O}(n)$), can solve very large problems and are easy to parallelize. The counterpart is that the choice of the iterative solver depends on the problem.

4. *post-processing procedures* extract the data of interest from the finite element solution and estimates the related errors.

[2] a matrix is ill-conditioned if the condition number is too large. This condition number measures how much the output value of the function can change for a small change in the input argument [3].

1.2 Pdetect

Pdetect is the software developed in the context of this work. In order to avoid to reinvent the wheel, *Pdetect* uses the *deal.ii* library to solve the Laplace equation [12]. This decision allows to rely on the optimized and robust code of *deal.ii* and to benefit from the cutting edge numerical methods this library provides.

deal.ii is a C++ library allowing to solve partial differential equations using the finite element method. It is a very powerful but low-level library. It offers several features such as adaptive meshes, grid handling and refinement, handling of degrees of freedom, input of meshes and output of results in graphics formats. Furthermore, *deal.ii* allows to easily write code that works for any dimensions because code using deal.ii is written independently of the space dimension. Thanks to this design choice, the code of our software is quite easily extensible to 3D.

The library allows to chose among several finite element method configurations. About *variational formulation*, it is possible to use the *discontinuous Galerkin method* [5], the *hybridizable discontinuous Galkerin method* [10] and much more. Furthermore, different *discretization strategies* can be implemented such as *hp-version* [9], *x-FEM* [15] and *isogeometric analysis* [13]. *deal.ii* also offers several solvers, both direct or iterative [11].

Finally, *deal.ii* supports multithreading as well as *MPI* [3]. Therefore, deal.ii is able to hardness the power of multithreaded CPUs as well as clusters composed of hundreds of computers. Consequently, the software developed in this thesis is multithreaded and could be extended to exploit the resources offered by clusters.

1.3 Weightfield

Weightfield is a program to study the performance of silicon and diamond detectors [16]. It simulates the energy released by particles in the detector and uses the Ramo's theorem to compute the signal current.

Weightfield allows to play with various parameters. Firstly, the user can select one of the following types of incident particle: minimum ionizing particle (MIP) with a uniform or non-uniform charge deposition of 75 electron-hole pairs per micron, MIP with non-uniform charge deposition and Landau distributed charge and a 5 MeV α particle. Secondly, *Weightfield* can simulate a magnetic field as well as thermal diffusion. Thirdly, the user can specify the material type (silicon or diamond) as well as the doping of the strip. Fourthly, following geometrical properties can be modified: the number of strips and the sensor thickness. Fifthly, the user can chose the bias voltage, the depletion voltage and control the gain layer. Finally, *Weightfield* is able to performs a simulation of the read-out electronic.

Weightfield has been used in this work to compare and valid the results obtained with our own software, *pdetect*.

[3] Message Passing Interface. MPI is used to develop distributed softwares running on top of clusters of computers.

1.4 Analytical solution of the weighting potential

The weighting potential has already been calculated for some type of geometry. Since *Pdetect* calculate the weighting potential, it is interesting to compare its results with the expression of the analytical solution.

In order to compare the results of *Pdetect* with the analytical solution, we have to introduce the context in which this solution was found. The Figure 1 shows the geometry in which the analytical solution has been calculated.

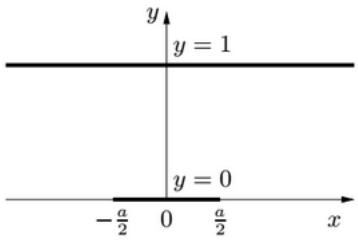

Figure 1: Detector geometry for the calculation of the analytical expression of the weighting potential [19]

After painful calculations, the solution of the weighting potential in the above situation has been calculated and is given by Equation 1.

$$\phi_w = atan\left(\frac{\sin(\pi y)\sinh(\pi\frac{a}{2})}{\cosh(\pi x) - \cos(\pi y)\cosh(\pi\frac{a}{2})}\right) \tag{1}$$

With this expression, it is not obvious to know the shape of the weighting potential in the two dimensional space. Therefore Figure 2 shows this weighting potential (It has been rotated by 90 degrees to compare more easily with the results of *Pdetect*).

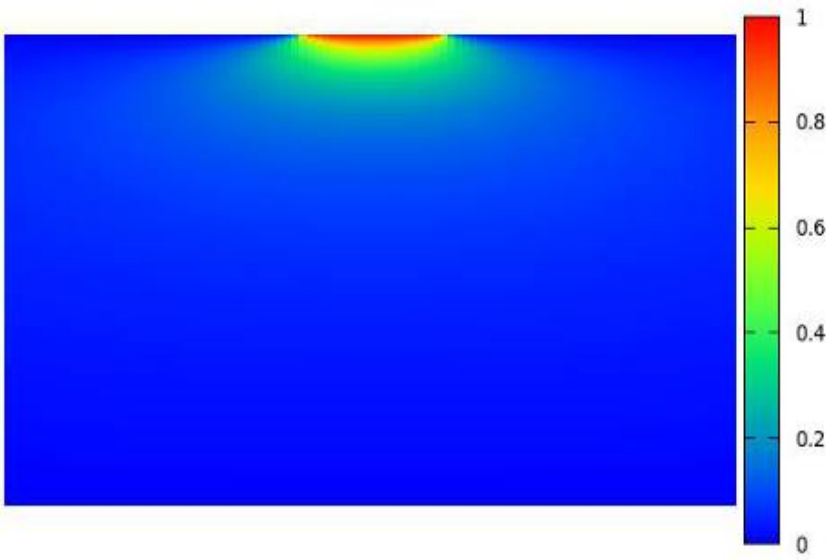

Figure 2: Two dimension plot of analytical solution of the weighting field given by Equation 1

On the figure above, it appears (as suggested by Figure 1) that the boundary conditions are free on the sides, and set to a zero potential the bottom (or on the top for Figure 1) and on top next to the strip. This is why we will use those kind of boundary conditions for the comparisons between the results given by *Pdetect* and the analytical solution.

2 Introduction to the physics of particle detectors

In this section, the concepts of particle detectors physics used in this project are introduced.

A particle detector is composed of a cathode, an anode and an active media between them (gas,...). A potential difference is applied between the cathode and the anode [17].

When a particle pass through the active media, the radiation ionizes the media molecules along the particle trajectory. Because of the applied potential difference, produced ion-electron pairs drift inside the detector until they reach the anode (for the ions) or the cathode (for the electrons). These ions and electrons are moving charges and therefore produce a current.

The number of ion-electron pairs per length n_{eff} produced in the media by the particle passage is given by the following formula:

$$n_{eff} = \frac{dE/dx}{w}$$

where dE/dx is the energy deposited by the particle in the media by unit of length, and w is the average energy to produce one ion-pair.

The charges drift in the detector media with a velocity function of the electric field and the mobility [20]:

$$|\vec{v}| = \mu|\vec{E}| \tag{2}$$

where μ is the *mobility*. Electrons and holes (or ions) have different mobilities. For example, in Silicon, mobilities are 1350 and 450 $cm^2V^{-1}s^{-1}$, respectively. In gas, the mobility difference between electrons and holes is much larger, electrons are typically a thousand times faster ($\mu =$ 100 $cm^2V^{-1}s^{-1}$ for electrons and $\mu = 0.1$ $cm^2V^{-1}s^{-1}$ for holes). Notice that the mobility is not a constant in general.

Due to saturation, the mobility decreases when fields of 104 Vcm^{-1} and higher are applied in the detector following the relation:

$$\mu_s = \mu \left(1 + \left(\frac{\mu|E_y|}{v_{sat}}\right)^{\beta}\right)^{-\frac{1}{\beta}} \tag{3}$$

where β is a constant, μ the mobility when not considering saturation, E_y the component of the electric field along the axis orthogonal to the anode and cathode, and v_{sat} the saturation velocity. The saturation velocity depends on the media and the temperature.

Once the velocity is known, the current generated by moving ion-electron pairs can be computed. The Shockley–Ramo theorem states that the instantaneous current generated by one moving charge q at velocity $\vec{v}$ is:

$$i = -q\vec{v} \cdot \vec{E}_w \tag{4}$$

where q is the signed charge and $\vec{E}_w$ is the *weighting field*. The weighting field is the electric field obtained when applying a potential of $1V$ to the measurement electrode and setting the potential of the other electrodes to $0V$.

The instantaneous current measured by the detector is the sum of the currents generated by the holes and electrons:

$$i_{tot} = \sum_{holes} i_h + \sum_{electrons} i_e \tag{5}$$

An additional effect to take into account when dealing with gas detectors is *charge multiplication* [17]. This effect multiplies the primary ionization charges by an avalanche phenomena. The *Townsend avalanche* is implemented in our software. It happens when the electric field is higher than 10^6Vm^{-1}. The electrons collide with the molecules of the media and, if their kinetic energy is sufficient, extract additional electrons from this molecules.

The Townsend avalanche multiplies the local number of electrons (and therefore the local electric charge) if the electric field is high enough and if the electrons are close to the cathode. When these conditions are fulfilled, during a time interval Δt the initial electric charge q_0 is multiplied according to the formula:

$$q = q_0 e^{\alpha \Delta x} \tag{6}$$

where Δx is the distance covered by the electron and α the *first Townsend coefficient*. This coefficient is computed as follows:

$$\alpha = ap\ e^{-bp/E}$$

where a, b are constants depending on the gas media, p the pressure in the detector (the atmospheric pressure is commonly used) and E the norm of the electric field at the charges position.

3 Software features

This section presents the features of the software. Firstly, the implemented detector geometries are presented. Secondly, some details about the resolution of the Laplace equation are provided. Thirdly, the computation of the current measured by the detector is described.

The software handles three types of 2D geometries:

1. `Middle circular holes rectangle`: this geometry is a rectangle with circular holes vertically centered and uniformly distributed along the horizontal axis (see Figure 1). The configurable values of the geometry are the rectangle width, the hole radius, the inter holes centers distance and the number of holes. The potential is set to $0V$ at the top and bottom boundaries. Left and right boundaries have free boundary conditions.

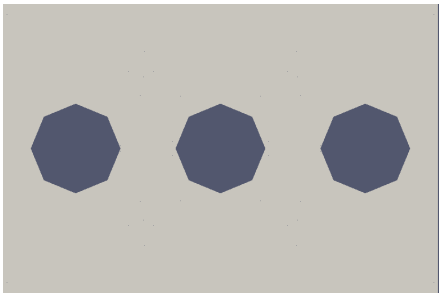

Figure 3: Middle circular holes rectangle geometry.

2. `Middle rectangular holes rectangle`: this geometry is a rectangle with rectangular holes vertically centered and uniformly distributed along the horizontal axis (see Figure 2). The configurable values of the geometry are the rectangle width, the number of holes, the inter holes distance, the hole width and the hole length. The potential is set to $0V$ at the top and bottom boundaries. Left and right boundaries have free boundary conditions.

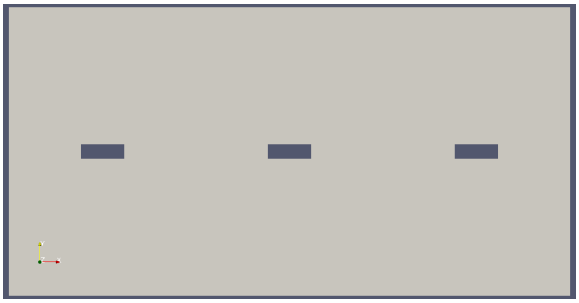

Figure 4: Middle rectangular holes rectangle geometry.

3. `Serrated rectangle`: this geometry is a rectangle with periodic holes inserted near the top boundary, along the horizontal axis (see Figure 3). The configurable values of the geometry are the rectangle width, the number of holes, the hole length (i.e. the length of the side parallel to the top rectangle boundary), the hole width and the inter holes space. These holes are the potential sources, the boundary value at their borders is therefore the strip potential. The holes inter-spaces have free boundary conditions. The right and left boundaries of the rectangle have free boundary conditions as well. Finally, the value at the bottom boundary is 0V.

Figure 5: Serrated rectangle geometry.

For each one of these geometries, a coarse grid (or mesh) is generated using functions of the `deal.ii` library.

Once the grid is generated (see Figure 6), the Laplace equation is solved for the considered geometry. This is achieved using all available CPU cores and in several iterations. At the first one, the grid is coarse and the error on the computed results is high. Then, the grid is refined only at cells with the largest errors and the Laplace equation is solved on this denser grid. This process continues until the error is smaller than a relative error provided by the user at each cell of the grid (see Figure 7). This is adaptive grid refinement. It allows to achieve good precision everywhere in the grid without losing time refining cells where the error is already small enough.

The adaptive refinement strategy used by *pdetect* can be compared with the uniform refinement strategy used by *Weightfield* looking at Figures 7 and 8. *Weightfield* uses a grid composed of 112500 cells whereas *pdetect* only requires a grid composed of 11966 cells to obtain results of similar precision simulating a detector with the following properties: width 300microm, strip length 75microm, potential 100V, pitch 300microm, strip number 1, maximum relative error on the potential for *pdetect* 0.9%. Notice that *Weightfield* always generates grids composed of 1microm×1microm cells.

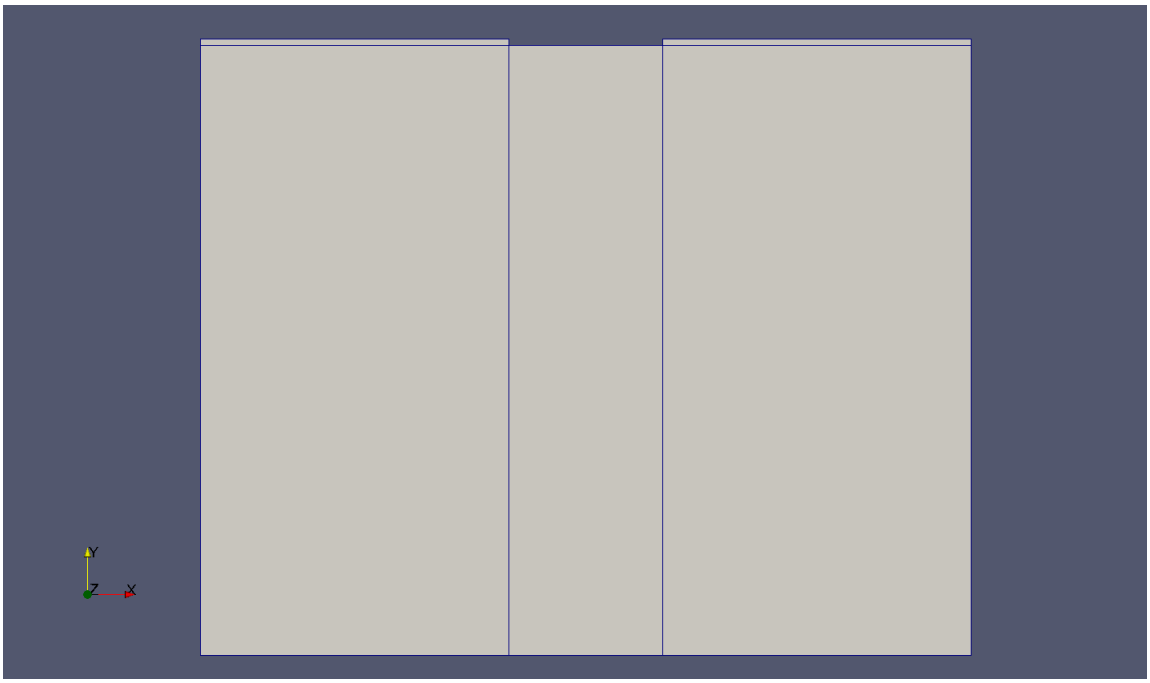

Figure 6: State of the initial grid before starting the potential computation for the serrated rectangle geometry with the following parameters: width 300microm, strip length 75microm, pitch 300microm, strip number 1. The grid is composed of 5 cells.

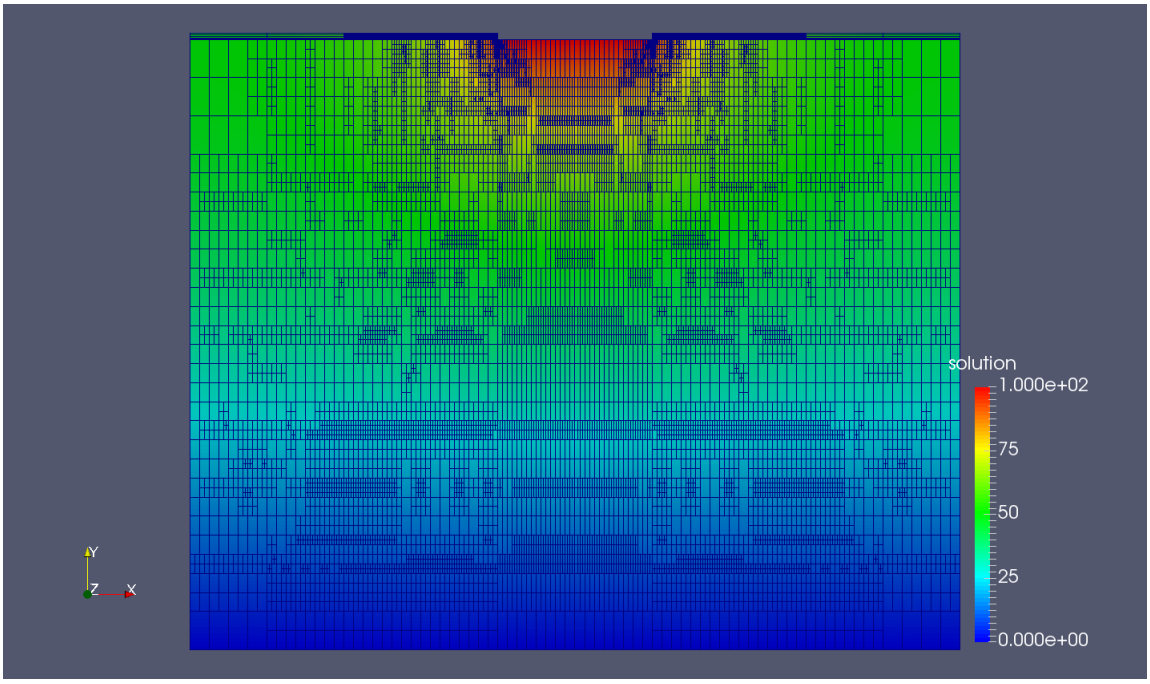

Figure 7: State of the grid at the end of the adaptive grid refinement. This grid has been obtained computing potential for the serrated rectangle geometry with the following parameters: width 300microm, strip length 75microm, potential 100V, pitch 300microm, strip number 1, maximum relative error on the potential 0.9%. The grid is composed of 11966 cells.

Figure 8: Grid used by *Weightfield* when computing the potential for the following geometry: width 300microm, strip length 75microm, pitch 300microm, strip number 1. The grid is composed of 112500 cells.

The result of the Laplace equation is of course the potential at each point of the grid. The gradient of the potential is available as well at the end of this process. A graphical representation of both the potential and its gradient can be written in a `vtk` file. These files can be read by the `Paraview` software.

The same process is performed with different boundary conditions in order to compute the weighting potential and the weighting electric field.

For each cell of the grid, the values of the potential, the error of the potential and the electric field are stored in a `rtree` data structure. In the algorithm computing the current measured by the detector, these three values have to be retrieved from the coordinates of a point. In order to retrieve the proper values, it is required to know to which cell the point belong. Since the grid is not uniformly refined, it is not easy to efficiently find this cell. Iterating through each cell of the grid is far too slow especially when 3D geometries will be introduced in the software. The algorithm finding the cell to which a point belong would have a $\mathcal{O}(n)$ time complexity, where n is the number of cells in the grid. The `rtree` data structure performs this search with a $\mathcal{O}(log(n))$ time complexity.

The software then uses these results to compute the current measured by the detector. The user has to specify the particle trajectory. Any trajectory is supported. The computation of the current is composed of the following steps.

Firstly, the ion-pairs generated by the particle pass are placed at their initial positions inside the detector. At this end, the intersections points between the detector boundaries and the particle trajectory are computed. Notice that a particle may enter and leave the detector several times (the potential sources, or strips, are not considered as being part of the detector). It happens for example if the particle trajectory is horizontal near the top boundary of a serrated rectangle geometry. The segments being part of both the particle trajectory and the detector geometry are

retrieved. The total distance covered by the particle inside the detector is then computed as the sum of the length of these segments. From this, the total number of ion-pairs created by the particle pass is computed as the product of the covered distance with the number of ion-pairs created by unit of length. The number of ion-pairs created by unit of length is considered as a constant and is different from one media to another. Depending on the precision level specified by the user, the total number of ion-pairs is uniformly spread along the path covered by the particle inside the detector. When the precision is higher, the total number of pairs is spread among more points. On the opposite, if the precision level is set to 0, all ion-pairs are placed at the same point.

Secondly, the charges are moved in the detector under the effect of the electric field. The speed of the charges is computed using Equation 2. Due to the saturation effect the mobility of charges may change depending on their position in the detector. Therefore, the mobility used in Equation 2 is computed using Equation 3 at each iteration.

The new position of the charge is simply:

$$(x', y') = (x + v_x \Delta t,\ y + v_y \Delta t)$$

The time interval Δt is automatically chosen by the software before each iteration depending on the maximum vertical speed of the charges:

$$\Delta t = \frac{w}{v_{y_{max}} c}$$

where w is the detector width, $v_{y_{max}}$ the maximum vertical speed among all the charges moving inside the detector at the previous iteration and c is a precision coefficient. This precision coefficient is a constant provided by the user. When the coefficient is greater, the time interval of the simulation is smaller and the results are more precise. Thanks to this adaptive Δt, the time interval is always sufficiently small. Using a constant Δt may be a problem dealing with gas detector, because the mobilities of the hole and the electron differ greatly.

For each time t, the current i is computed using the Equations 4 and 5. Each pair (t, i) is saved in a vector which can be written to a file at the end of the simulation.

At the end of each iteration, the electric charge at one point in the detector may be multiplied due to the Townsend avalanche effect following Equation 6. Notice that this effect happens only for gas detectors.

4 Discussion and applications

In this section we will firstly discuss the results given by the program developed for this work, *Pdetect*, and compare it with an analytical solution that will be introduce later. After that, we will talk about three different applications, one with a silicon detector and two with a gas detector, and compare the results of the computed current with the current computed by *Weightfield*.

For the entire section, the type geometry of the detector used in *Pdetect* is a serrated rectangle (see Figure 3).

4.1 Comparison with the analytical solution

As said earlier, we will compare here the weighting potential computed by *Pdetect* and the analytical solution given by Equation 1. To do so, the boundary conditions used for the computation by *Pdetect* in this section are similar to the boundary conditions used to compute the analytical solution (see Figure 9).

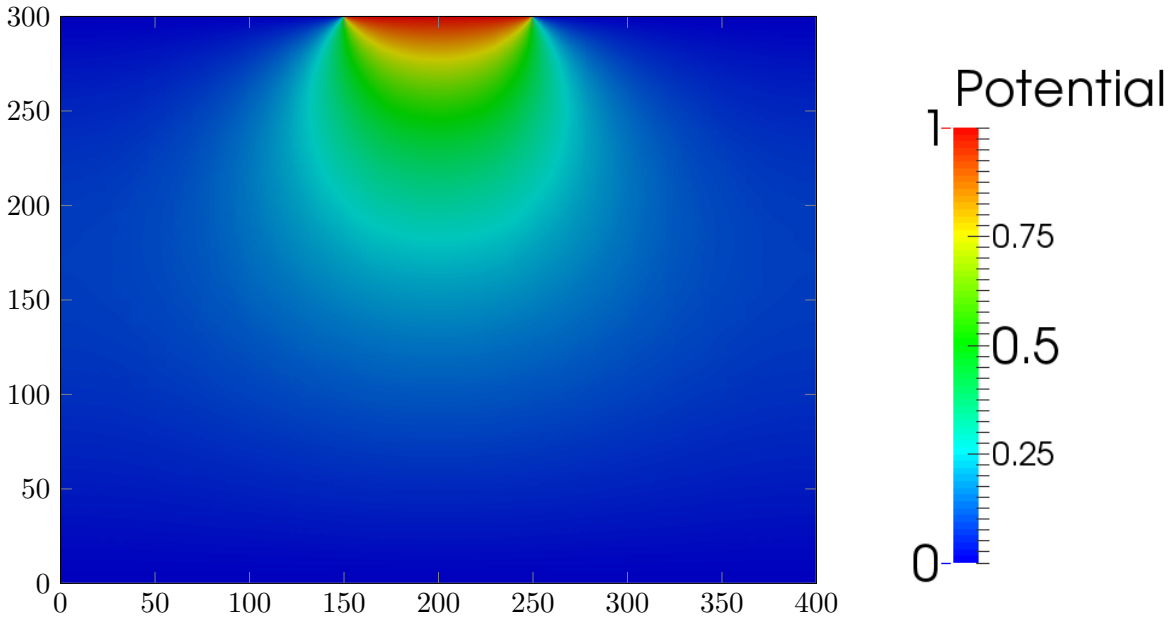

Figure 9: Weighting potential inside a serrated detector given by *Pdetect* with pitch of 400μm, strip length of 100μm, detector width of 300μm, free boundary conditions on the side of the detector.

Now that the boundary conditions are the same in the analytical case and for *pdetect*, the comparison of the weighting potential should be relevant.

Figure 10 shows both the weighting potential computed by *Pdetect* and by using Equation 1 along a straight vertical line passing just in the middle of the srip.

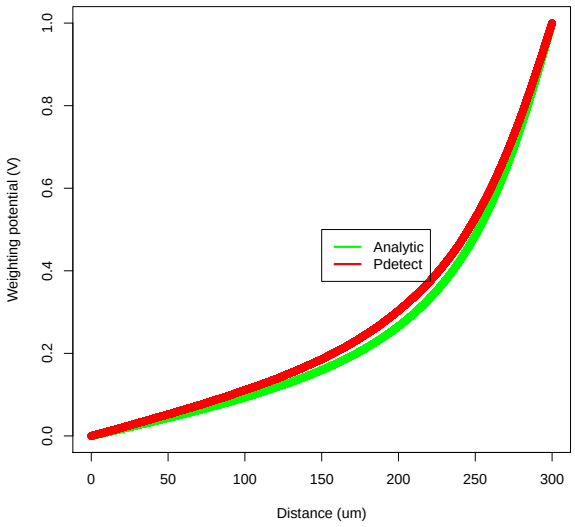

Figure 10: Weighting potential along a vertical line passing in the middle of the detector with pitch of 400μm, strip length of 100μm, detector width of 300μm, free boundary conditions on the side of the detector.

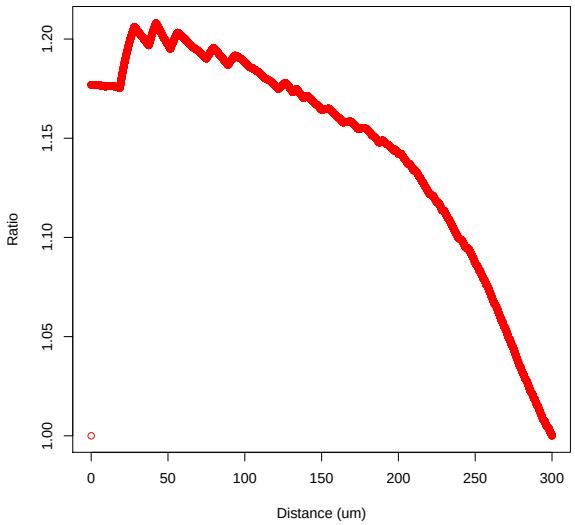

Figure 11: Ratio between the weighting potential along a straight line computed by *Pdetect* and the analytical solution for a detector with pitch of 400μm, strip length of 100μm, detector width of 300μm, free boundary conditions on the side of the detector.

It clearly seems to have some correlation between the two. By changing the dimension of the detector in *Pdetect*, the graph will change a little bit and can be closer or further to the graph of the analytical solution.

Unfortunately, since we do not have more information about the context in which the equation 1 has been computed (the exact geometry), it is not possible to make a real better comparison. However, a better comparison between *Pdetect* and the analytical solution is made in the appendix (see Appendix A).

4.2 Comparison with *Weightfield*

Now that the comparison with the analytical solution is done, it would be interesting to compare the results of *Pdetect* with the results of *Weightfield* since it is another simulation of particle detector program, already use in some experiments.

Firstly, it is important to see that the boundary conditions used in *Weightfield* are not the same than those used for the computation of the analytical solution. The Figure 12 shows the weighting potential inside the detector, simulated by *Weightfield*.

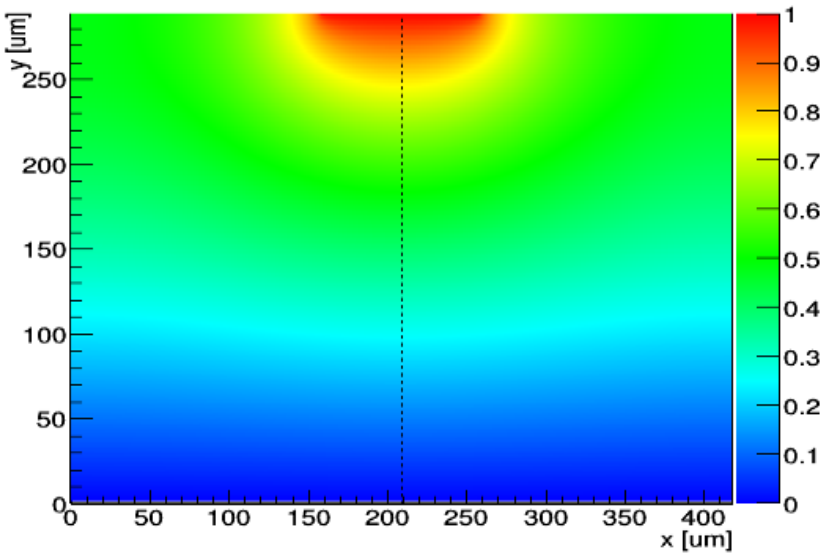

Figure 12: Weighting potential inside the detector, given by *Weightfield* with pitch of 400μm, strip length of 100μm, detector width of 300μm.

The Figure 12 clearly shows that the boundaries are free not only on the side of the detector, but also on the top of it, next to the strip.

Since Weightfield is used and trusted in actual experiments, it seems relevant to use the same kind of boundary conditions in *Pdetect* (see Figure 13).

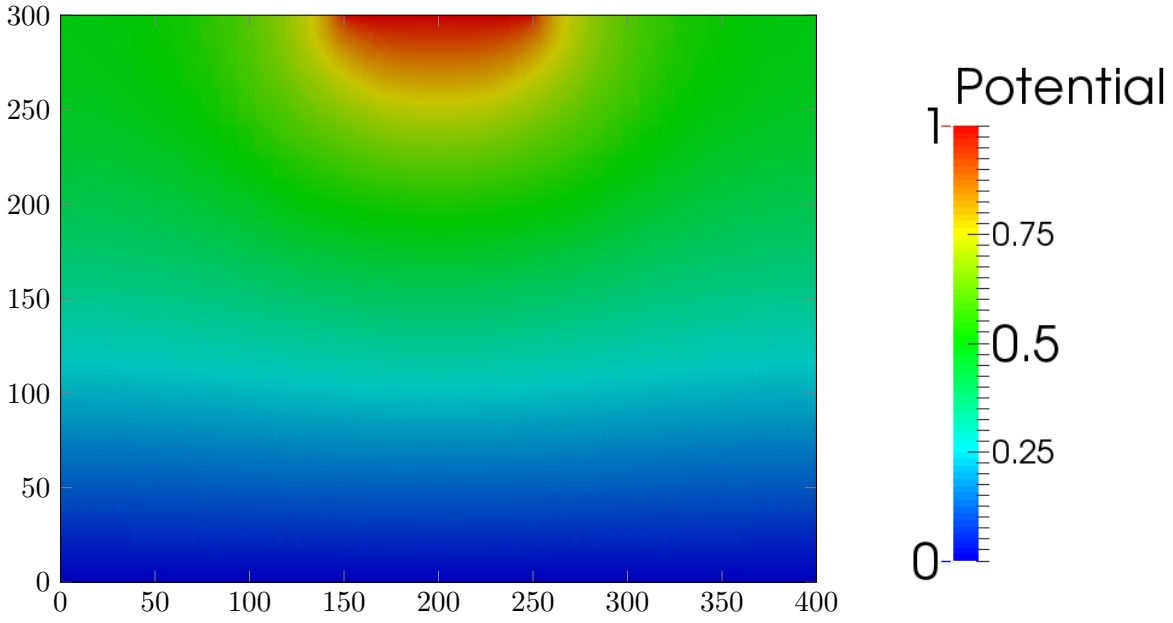

Figure 13: Weighting potential inside the detector, given by *Pdetect* with pitch of 400μm, strip length of 100μm, detector width of 300μm.

Now we have the same boundary conditions for *Pdetect* and *Weightfield*. We can therefor make a

relevant comparison between both. Figure 14 and Figure 15 show the weighting potential computed along a straight vertical line passing in the middle of the detector by *Weightfield* and *Pdetect* respectively.

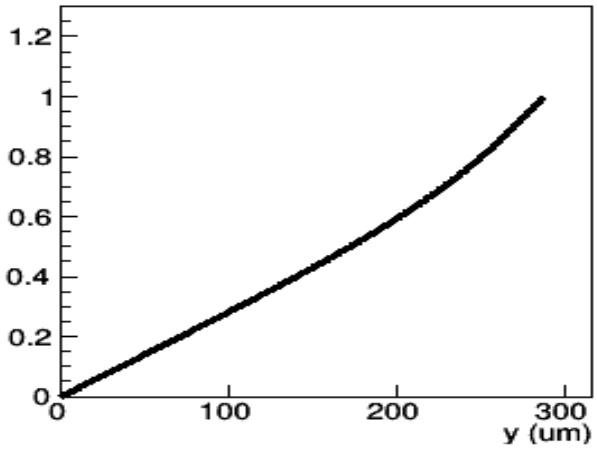

Figure 14: Weighting potential along a vertical line passing in the middle of the detector, given by *Weightfield* with pitch of 400μm, strip length of 100μm, detector width of 300μm.

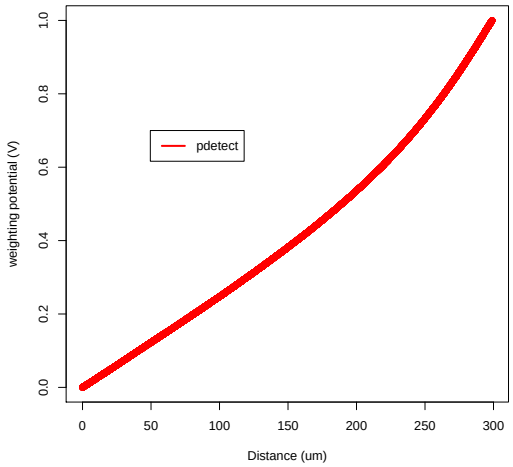

Figure 15: Weighting potential along a vertical line passing in the middle of the detector, given by *Pdetect* with pitch of 400μm, strip length of 100μm, detector width of 300μm.

On those graphs, it appears that even if the weighting potential of *Pdetect* is quite different of the analytical solution, it is still very similar to the weighting potential of Weightfield (unfortunately since we can't have the data used to make the graph of *Weightfield*, we cannot plot the ratio to properly see the concurrence).

This is why for the rest of this work, the free boundary conditions will be used.

4.3 Applications

In this section we will talk about three applications of our program. Firstly we will talk about the simulation of a silicon detector, then the simulation of two cases of an gas detector, each with their own properties.

We will compare our results with known results, and for the silicon we will also compare it with Weightfield, which can simulate a silicon detector.

4.3.1 Silicon detector

The silicon detector was the first type of detector that was implemented.

For the application on the silicon detector, we used a serrated and rectangular detector (see Figure 3) using realistic dimensions and voltage. In order to use the silicon type for the running of the program, the user have to specify it by using a macro define in the file `Constants.hpp`.

The silicon detector uses all the features provided by the program, except the Townsend avalanche, which is unique to gas detectors.

Different constants

In order to contextualize the results shown below, it is necessary to first set the different constants used in the equations of the Part 2 of this thesis. All the constants introduced below takes those values only for the case of a silicon detector, of course.

- w = 3 eV : w is the average energy to produce one ion-pair.
- $\mu_e = 1350\ \mathrm{cm^2V^{-1}s^{-1}}$: μ_e is the mobility of the electrons when not considering saturation.
- $\mu_h = 450\ \mathrm{cm^2V^{-1}s^{-1}}$: μ_h is the mobility of the holes (ions) when not considering saturation.
- $v_{sat} = 8{,}37{*}10^4\ \mathrm{ms^{-1}}$: v_{sat} is the saturation velocity (this value is taken from the code of *Weightfield* [16]).

We do not need the values of the other constants used in Part 2 since those are for the Townsend avalanche which don't apply here.

To be fully consistent, we also need the dimensions of our detector:

- Detector width = 300 μm : The width of the detector.
- Strip length = 25 μm : The length of one strip (where the potential is applied).
- Pitch = 100 μm : The distance between the middle of a strip and the middle of the next one.
- V_b = 100V : The bias voltage applied.
- V_d = 50V : The depletion voltage applied (*Pdetect* doesn't use it, we only need it in *Weightfield*).

Results

Let's now talk about the results given by the program and let's compare them with *Weightfield*.

The program *Pdetect* simulates the induced current on the strips when a particle passes through it. For those results we are using a detector with only one strip and a particle passing vertically right in the middle of it, both in *Pdetect* and in *Weightfield*, to have a better comparison. The Figure 16 shows both the current simulate by *Pdetect* and *Weightfield*. Figure 17 shows the ratio between them.

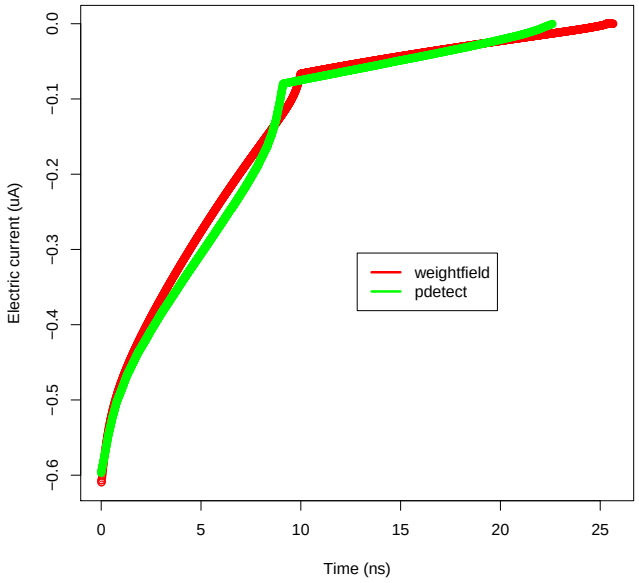

Figure 16: Current induced by a particle in function of time, in a silicon detector, computed by *Pdetect* and *Weightfield*.

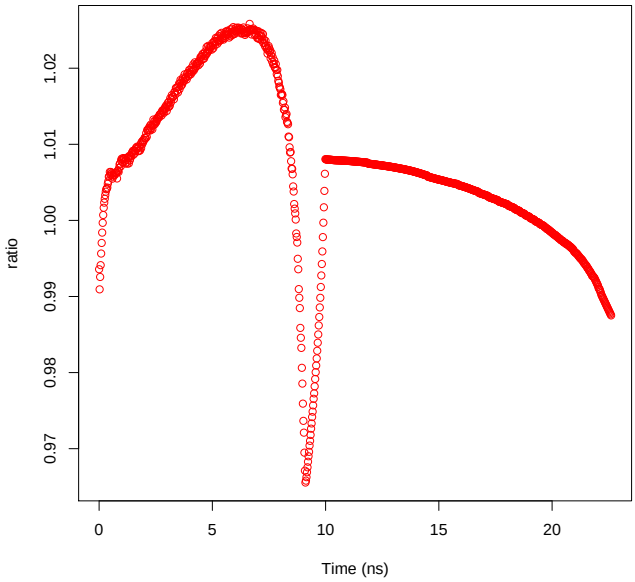

Figure 17: Ratio of the current induced by a particle between *Pdetect* and *Weightfield*

By taking a closer look, we see the total time taken for the generated ion-pairs to move to the edges of the detector is exactly 22,6056ns for *Pdetect* and 25,28ns for *Weightfield*. Also the maximum currents are respectively -0,596511μA and -0,606824μA. Plus there are clearly some slight differences in the two graphs. Those differences are due to some effects featured in Weightfield but not in *Pdetect* such as the depletion voltage or the gain.

Indeed, the number of ion-pairs generated by the pass of particle in *Pdetect* and in *Weightfield* are respectively 22275 pairs and 21222 pairs. Such a small difference wouldn't justify the difference of current induced, especially since *Weightfield* has a bigger maximum current but less ions-pair generated.

4.3.2 Gas detector

The gas detector is the second type of particle detector implemented. The mechanics are basically the same as for the silicon detector, the detector is also a serrated and rectangular detector (see Figure 3). The only real difference is the use of the Townsend avalanche for the the helium detector (or for any other gas detector). In those applications, we will use an helium detector.

Once again the user can use the helium detector by using a macro defined in the file `Constants.hpp`.

Different constants

Since it is another type of detector, it has its own properties and therefore the constants used for the silicon detector may not be used. We thus redefined the constants used in the equations of Part 2 for the case of helium detector and define the constants used for the Townsend avalanche :

- w = 100 eV
- $\mu_e = 100\ \mathrm{cm^2V^{-1}s^{-1}}$
- $\mu_h = 0.1\ \mathrm{cm^2V^{-1}s^{-1}}$
- $v_{sat} = 50\ \mathrm{ms^{-1}}$: v_{sat}
- p = 1 atm : The pressure inside the detector.
- $a = 3\ \mathrm{Torr^{-1}cm^{-1}}$: A constant used in the computation of the first Townsend coefficient (taken from the lesson of Eduardo Cortina Gil [17]).
- $b = 34\ \mathrm{VTorr^{-1}cm^{-1}}$: Another constant used in the computation of the first Townsend coefficient (taken from the lesson of Eduardo Cortina Gil [17]).

For the helium detector we will make two applications by simply changing the dimensions of the detector.

The first application will use those dimensions :

- Detector width = 5mm
- Strip length = 0,9cm
- Pitch = 1cm
- V_b = 10000V

And the second application will use those :

- Detector width = 3cm
- Strip length = 100 μm
- Pitch = 1cm
- V_b = 2000V

Results

For the helium detector, there are no comparisons with *Weightfield* since it doesn't simulate any gas detector. The comparisons will thus be done with known results.

We will begin by the first case and discuss about the second later. The resulting current simulated by *Pdetect* for the first case is shown on Figure 18 (The particle passes again vertically in the middle of the strip).

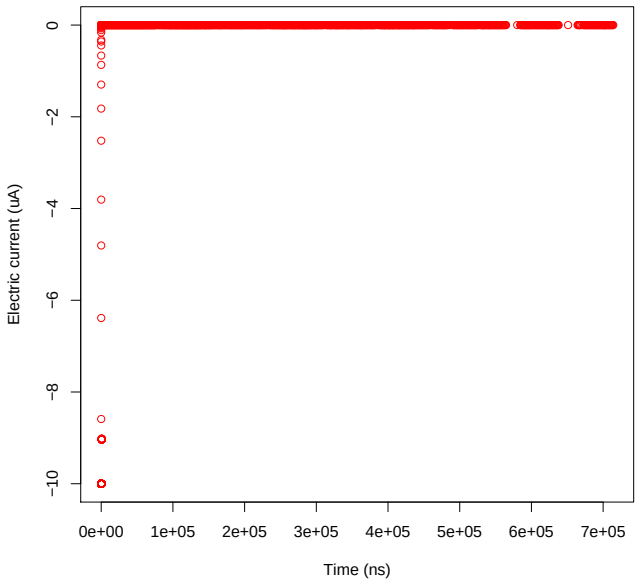

Figure 18: Current induced by the ion-electron pairs in function of time, in the first case of helium detector.

It seems, on the graph, to have a peak of current when the particle deposit the charges in the detector which fade almost instantly. Actually that is not what happens. This peak of current is the result of the electrons moving towards the detector to reach the cathode. But since those electrons are way quicker than the holes (almost a thousand times quicker), they will reach the cathode long before the holes reach the anode. Once the electrons are all at the cathode, only holes remain in the detector. Due to their slowness, they induce a current so small compare to the current that was induced by the electron that it seems on the graph to have no current.

The Figure 19 shows the current induced only by the electrons (by simply zooming on this part in the Figure 18).

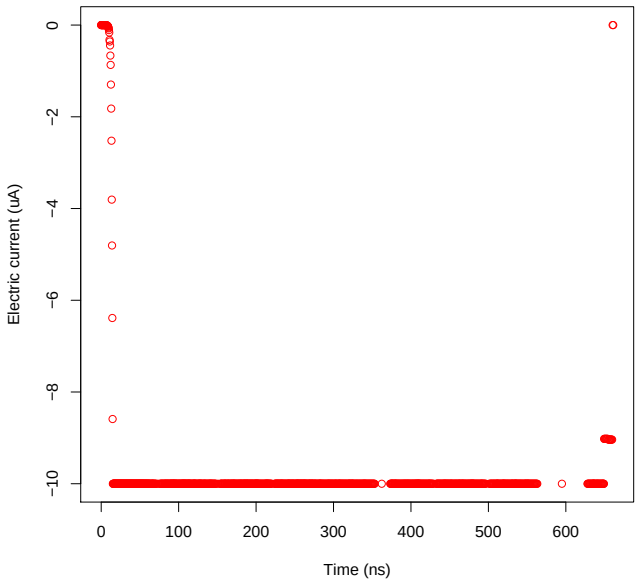

Figure 19: Current induced by the electrons in function of time, in the first case of helium detector.

Now it is clear that this peak of current didn't fade instantly. Instead, there is now a weird plate on the graph which wasn't there for the silicon case. Why?

This is due to two effects: the Townsend avalanche, and the electronics in the detector. Indeed, on the graph there is firstly an increasing current, due to the fact that while the electrons are moving toward the cathode, they have enough energy to create a new ion-electron pair. This is the Townsend avalanche. This phenomena occurs when the electric field inside the detector exceeds 10^6V/m, which is the case in this particular application, where the electric field is $\pm 2 * 10^6$V/m.

The presence of a plate on the graph is due to the electronics inside the detector. The electrodes in which the current is induced cannot handle a very high current, it will have a limit current that can't be surpassed. In this work (in the program), we introduced this value manually, and fixed it the limit current to 1μA, which seems reasonable. The reason why the current here exceed this limit, is because of the Townsend avalanche (without any limit, the induced current reaches $\pm$1A).

To check the validity of the results, let's compare those at some already known results. With the dimensions of the first application of helium detector, the particle generates only 4 ion-electron pairs (3,9 to be precise). The detector being half a centimeter thick, the particle thus generates between 7,8 and 8 ion-pairs per centimeter. This result is totally realistic, using the lesson of Eduardo Cortina Gil [17], we see the theoretical number of ions-pairs in a helium detector is 7,8 ion-pairs per centimeter. We can therefore assume that the results given by *Pdetect* are accurate.

Let's now talk about the second case of helium detector. The graph of the induced current is shown on Figure 20.

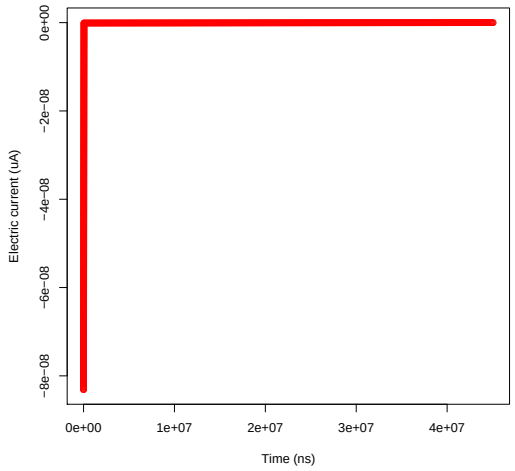

Figure 20: Current induced by the ion-electron pairs in function of time, in the second case of helium detector.

Once again the graph isn't very explicit due to the slowness of the holes compared to the electrons. Figure 21 shows the current induced by the electrons only (once again, it's only a zoom from Figure 20).

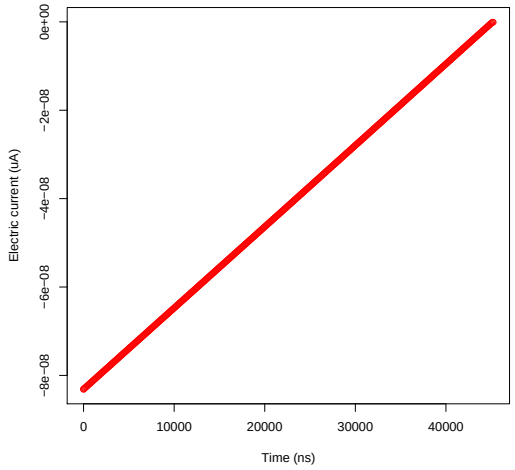

Figure 21: Current induced by the electrons in function of time, in the second case of helium detector.

The graph looks now a bit more like the current induce into a silicon detector. Actually, there is no Townsend avalanche here since the electric field is too small to generate it. But here, unless like for the silicon, the current decrease steadily. This is because in this particular application, is almost null everywhere. Therefore the electrons are almost not accelerated.

Conclusion

In this work, a software computing the current induced by the pass of a particle in a detector has been developed.

This work allows us to derive the following conclusions. The finite element method, and in particular its implementation in the *deal.ii* library, is an accurate and efficient way to solve the Laplace equation for the considered geometries. The solution is considered accurate since it is very close to both the analytical solution for carefully chosen parameters and the solution provided by *Weightfield*. About efficiency, it only takes between a few seconds and one minute for our software to solve the Laplace equation.

Another conclusion is that using adaptive grid refinement strategy instead of a uniform grid does not noticeably affect the results. Moreover, for the considered 2D geometries, the speedup offered by adaptive grid refinement over using a uniform grid is not significant. However, this speedup is expected to grow sharply when dealing with much more heavy 3D grids.

This work also shows that the boundary conditions have a significant impact on the computed potential. Indeed, enforcing Dirichlet boundary conditions setting the non-strip detector boundaries to 0V or instead enforcing Neumann boundary conditions setting a null derivative at these boundaries provides very different results.

A last conclusion about the potential computation is the influence of the number of strips on the weighting potential. The weighting potential computed for a one strip detector is very different from the one computed for a three strips detector. Conversely, the weighting potentials computed for three and five strips detectors are identical.

The computation of the current induced by a particle was found to be the most heavy computation. Without any optimization, i.e. accessing the potential and electric field at one cell with a $\mathcal{O}(n)$ time complexity, n being the total number of cells in the grid, the computation was far too slow. This process has been sped up using a *rtree* data structure which allows to access data of interest with a $\mathcal{O}(\log n)$ time complexity. This computation nevertheless remains the one taking the most time to complete. It takes typically four or five times the time required to solve the Laplace equation (a few minutes). This computation should scale well when passing to 3D geometries thanks to the logarithmic time complexity. It is expected that the potential computation becomes the slowest phase when handling 3D geometries since its time complexity is far worst than logarithmic (at best $\mathcal{O}(k \log k)$, k being the size of the finite element method matrix [18]).

The currents obtained for silicon detectors are comparable to the results of *Weightfield*, another simulation software. The difference are at most $\approx$10%. This difference does not come from differences in the computed potentials since they appear to be identical. It is unlikely that it is due to differences in the electric fields since it is just the the opposite of the potential gradient. Authors believe the differences are explained by the additionnal physical effects handled by *Weightfield*. For example, the number of initial holes and electrons are different in *Weightfield*. This behavior is not implemented in *Pdetect* yet. Moreover, *Weightfield* takes into account additional parameters such as the temperature and the depletion voltage. It would be interesting to compare the two softwares again once missing physical effects are implemented in *Pdetect*.

The results obtained for gas detectors still need to be validated. The implementation of the Townsend avalanche leads to abnormally high currents ($\approx 10^{80}$A). Authors are confident in the correctness of the implementation regarding the equations of the Townsend avalanche. The issue

may come from the lack of a mechanism to stop the avalanche once there are no electrons left to extract. Tests have been performed limiting the number of free electrons in the detector. Results are in this case not interesting since the maximum allowed current is reached very quickly. Further investigation need to be made on this behavior.

Another flaw in this work is that the finite element method parameters used by our *deal.ii* code are unknown. This code is very low level and is inspired from the *deal.ii* tutorial [4]. Therefore, it is not easy for people inexperienced with finite element method to make the connection between the *C++* code and the finite element method concepts it implements. However, since the Laplace equation is very common and in view of the consistent results, authors are confident in the solution of the Laplace equation. Using finite element method as a black box does not alter the quality of this work. Maybe experienced finite element method users may find ways to improve the process. However, authors do not see it as a priority since the current code is already efficient and accurate enough to answer current needs.

This work is a first step to the development of a properly designed and open source software to simulate particle detectors. Authors are confident in the results for silicon detectors and gas detectors when there is no Townsend avalanche. Conversely obtained results for gas detectors with Townsend avalanche are false and the simulation of this phenomena needs to be corrected in order to match the physical reality. Although there are still many features to introduce in the software, authors believe it is a solid basis for further improvements.

Future work

There are a lot of ways to improve and extend the developed software.

Authors highlight five new features that could be introduced. Firstly, the computation of the current for the rectangular geometry with circular holes could be implemented quite easily. Secondly, additional physical effect could be implemented such as the *Geiger avalanche*. Thirdly, additional 2D geometries could be introduced such as rectangular potential sources but with gaussian curves at their corners. Fourthly, the software can be extended to handle both 2D and 3D geometries. Fifthly, a graphic user interface could be developed to ease the usage of the software. Sixthly, the implementation of the Townsend avalanche phenomena must be improved to match the real behavior of gas detectors.

Furthermore, since the passage to 3D geometries will slow down the computations, it may become interesting to modify the `deal.ii` code in the `LaplaceSolver` class in order to run the software on clusters. Research could also be performed on how to efficiently parallelize the computation of the current among several CPU cores (the finite element method is multithreaded but the current computation is not for now) or among nodes of a cluster. Another performance improvement would be to offload some computations on Graphics Processing Unit.

Finally, the results obtained for gas detectors (helium) must be validated by comparing them with experimental measurements or results provided by other simulation softwares.

A Comparison between the analytical and numerical solutions

In this section of the appendix, we will continue the discussion of the comparison between the results of *Pdetect* and the analytical solution given by Equation 1 (see Section 4.1).

To continue this comparison, we will compare the weighting potentials along different line. We have already made the comparison for a straight line passing vertically in the middle of the detector. On Figure 22, the graphs show the values of the weighting potentials along a straight and vertical line, but this time passing right in the middle of the left border of the detector and the left border of the strip (Figure 23 shows the ratio).

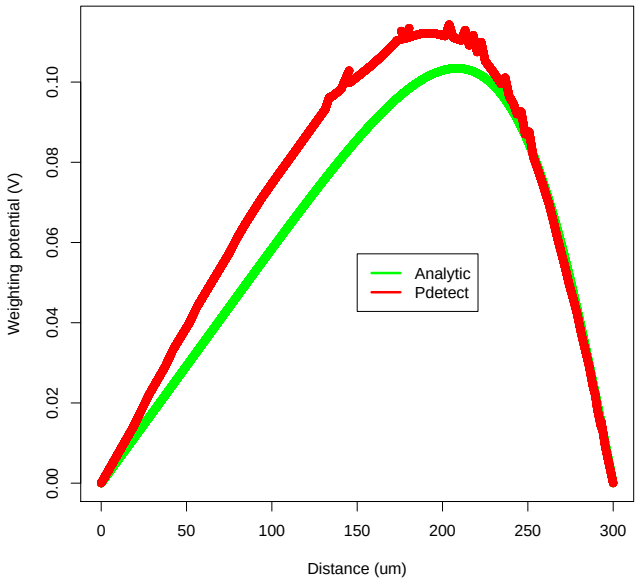

Figure 22: Weighting potential along a straight vertical line passing between the strip and the border of the detector with pitch of 400μm, strip length of 100μm, detector width of 300μm, free boundary conditions on the side of the detector.

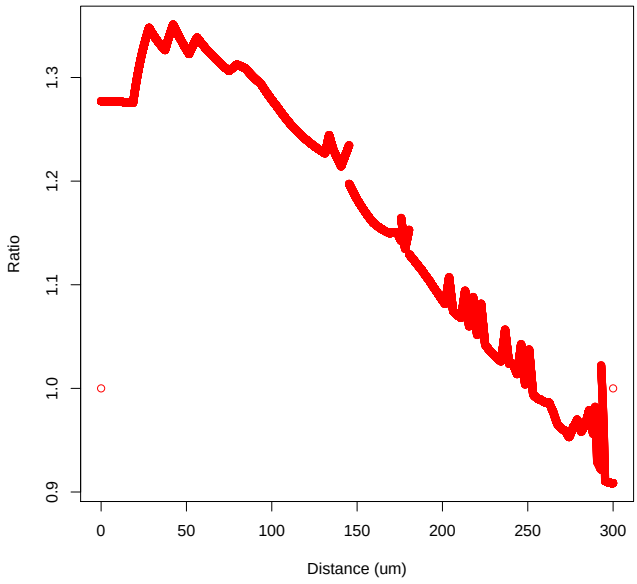

Figure 23: Ratio of weighting potentials along a straight vertical line passing between the strip and the border of the detector with pitch of 400μm, strip length of 100μm, detector width of 300μm, free boundary conditions on the side of the detector.

On those graphs, there are some difference between the results of *Pdetect* and the analytical solution. But this graph is for one specific geometry of detector in *Pdetect*. Indeed, by simply changing the dimensions of the detector, the graph will fit more (or less) with the graph of the analytical solution. Once again the lack of knowledge about the specific conditions in which the analytical solution has been calculated is a bit problematic.

Anyway, even if the differences seem big, by looking at the scale, there actually rather small than big. Let's still continue the comparisons by plotting the weighting potential along a vertical straight line, now passing right at the edge of the strip. This particular case is very interesting since on there are a singularity at the edge of the strip. Indeed, the strip itself have certain potential (1V in this case), but just next to it, outside the strip, the potential is set to zero (with the boundary

conditions of the analytical solution). Figure 24 shows the potential along this line, for both *Pdetect* and the analytical solution (Figure 25 shows the ratio).

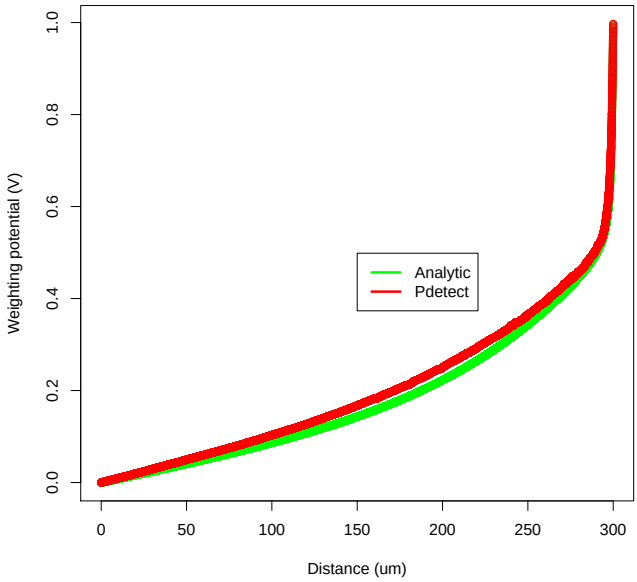

Figure 24: Weighting potential along a straight vertical line passing right at the edge of the strip with pitch of 400μm, strip length of 100μm, detector width of 300μm, free boundary conditions on the side of the detector.

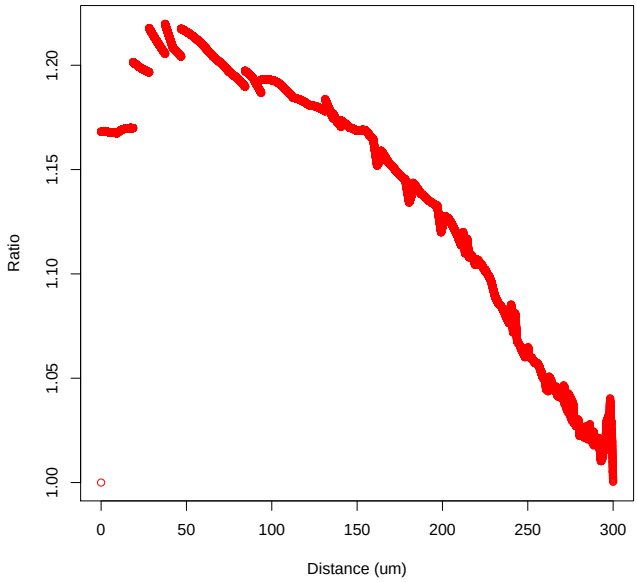

Figure 25: Ratio of weighting potentials along a straight vertical line passing right at the edge of the strip with pitch of 400μm, strip length of 100μm, detector width of 300μm, free boundary conditions on the side of the detector.

Here the two graphs seem to fit almost perfectly, which is a very good sign for *Pdetect*. But again, the graph of *Pdetect* can change a little bit by changing the dimensions of the detector.

Now all interesting cases of vertical line have been compared. Let's now look at the weighting potential along a horizontal line, passing just below the strip (see Figure 26 and Figure 27).

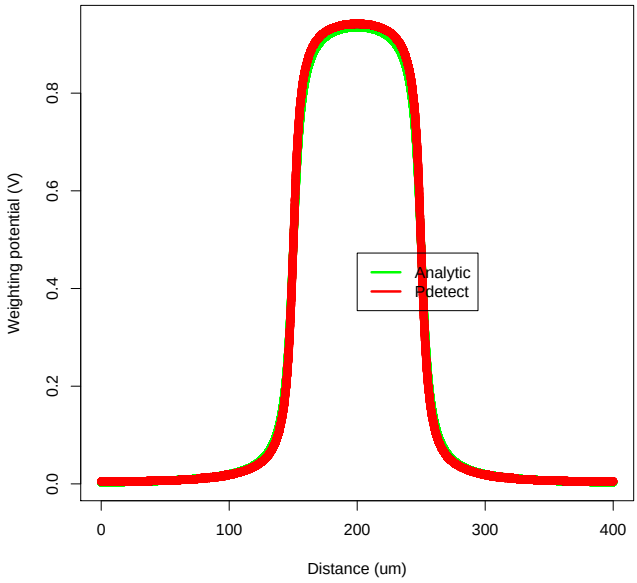

Figure 26: Weighting potential along a straight horizontal line passing right below the strip with pitch of 400μm, strip length of 100μm, detector width of 300μm, free boundary conditions on the side of the detector.

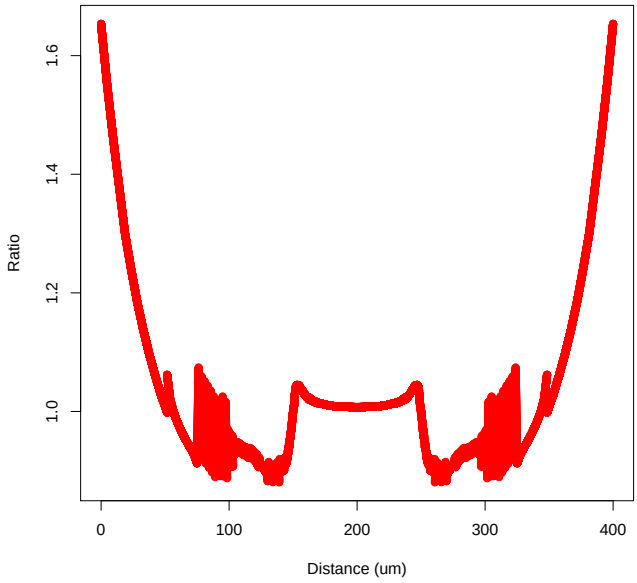

Figure 27: Ratio of weighting potential along a straight horizontal line passing right below the strip with pitch of 400μm, strip length of 100μm, detector width of 300μm, free boundary conditions on the side of the detector.

As for the previous ones, the graphs are quite similar.

Let's now make a last comparison between the results of *Pdetect* and the analytical solution. Figure 28 shows the weighting potentials along an oblique straight line, passing right at the center of the detector (Figure 29 shows the ratio).

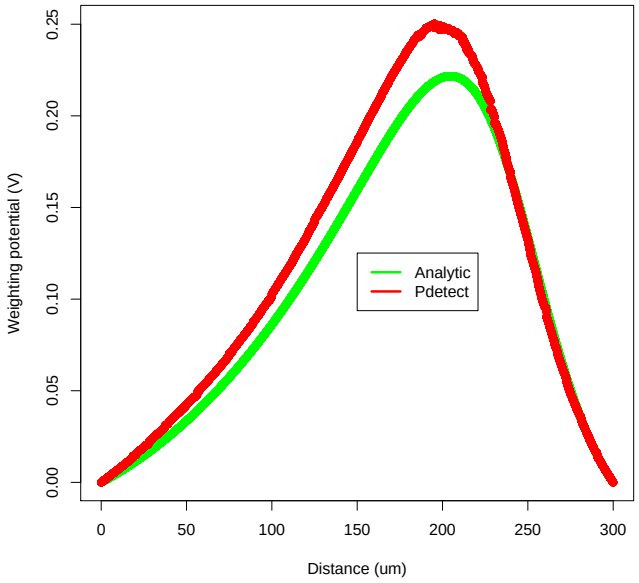

Figure 28: Weighting potential along a straight oblique line passing right in the center of the detector with pitch of 400μm, strip length of 100μm, detector width of 300μm, free boundary conditions on the side of the detector.

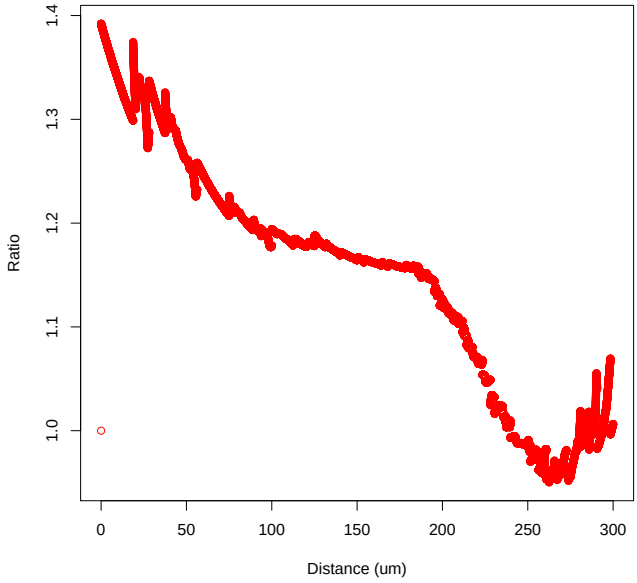

Figure 29: Ratio of weighting potential along a straight oblique line passing right in the center of the detector with pitch of 400μm, strip length of 100μm, detector width of 300μm, free boundary conditions on the side of the detector.

On those graphs, there is a slight difference between *Pdetect* and the analytical solution, but as always, the graph can change a bit by changing the dimensions of the detector in *Pdetect*.

All those comparisons tends to validate the results computed by *Pdetect*. Indeed, even if there are some differences, those are really small and can be reduced by changing some parameters in *Pdetect*.

B Software architecture

This software is developed in C++ with the object-oriented programming paradigm. This section firstly presents how the final software should be organized in several modules. Secondly, the most important classes and their responsibilities are presented. Relevant implementation details are also mentioned.

B.1 Model–view–controller (MVC) software architectural pattern

The program main function calls functions from the `test` folder. These functions assemble the different objects to perform the required computation. In the final version of the program, functions of the test folder should be replaced by a graphic user interface: a `view` and a `controller` following

the model-view-controller software engineering pattern. In this pattern code related to core of the program functionality (the `model`: mathematical computations, file access,...) is separated from the code related to the user interface (the `view`). The `view` and the `model` are connected by the `controller` module.

The main advantage of this design pattern is to be able to change the user interface without performing any modification to the code of the `model` module. Furthermore, mixing model and graphic interface related code should be avoided because it leads to less readable and not modular code.

The graphic user interface would allow the user to specify parameters of the simulation at runtime rather than hardcoding parameters directly in the functions of the `test` folder. The development of the `controller` and `view` modules is left for future work.

B.2 The model module

The reminder of this section presents the most important classes included in the `model` module.

The `MyGridGenerator` class provides functions to generate `deal.ii` grids (i.e. objects of type `Triangulation` handled by `deal.ii`) for supported geometries. This class heavily relies on functions of the `deal.ii` library. A common strategy is to first generate little rectangles using the `hyper_rectangle` method from the `deal.ii GridGenerator` class and assemble them using the `merge_triangulations` method from the same class to obtain the desired grid. Developers led to build methods to generate new geometries must be aware that the `merge_triangulations` method requires the merged triangulations to have common vertices at the boundaries where the two triangulations are adjacent, otherwise the boundaries of the geometry may not be well defined, leading to strange behavior when solving the Laplace equation.

The `MyGeometryInfo` abstract class provides informations related to the geometry of the detector as well as methods to compute the intersections of a line with the boundaries of the geometry and to check if a point is inside the geometry. This abstract class has three implementations: one for each geometry introduced at Section 3.

The `LaplaceSolver` class responsibility is to solve the Laplace equation. The whole code related to finite element method resides in this class. Its constructor is presented at Listing 1.

```
LaplaceSolver(Triangulation<dim> *triangulation,
double refine_accuracy, unsigned max_iter, double stop_accuracy,
const Function<dim> *right_hand_side,
BoundaryConditions<dim> *boundary_conditions,
bool constraints_are_periodic)
```

Listing 1: Constructor of the `LaplaceSolver` class.

The `triangulation` parameter is a pointer to a grid generated using methods of the `MyGridGenerator` class. The `refine_accuracy` is the maximum error tolerated at each cell. For a given grid (fixed refinement level), the `stop_accuracy` is a stop criteria that indicates if the solver has reached convergence. If the error difference between two successive iterations of the solver is less than

`stop_accuracy` the solver stopped iterating on the current grid. Notice that it does not mean that the computation of the Laplace equation is over: the solver may solve the equation on finer grids afterwards until the error is less than `refine_accuracy` everywhere in the grid. The solver also stopped when the number of iteration on a given grid is equel to `max_iter`. The `right_hand_side` parameter is the function f at the right side of the Poisson equation:

$$\nabla^2\phi(x,y) = f(x,y)$$

Since in this project the Laplace equation is solved, `right_hand_side` simply refers to the trivial constant function $f(x,y) = 0$ for all $(x,y) \in R^2$. The `boundary_conditions` parameter is a function called by the Laplace equation solver on each point of the domain boundary for which the free boundary conditions are not enabled. Boundary values are encoded in this function.

The functions that dictates the boundary values are stored in the `boundary_conditions` folder. There are two functions for each type of geometry: one provides boundary values for the potential and the electric field computation, the other one for the weighting potential and the weighting electric field computation.

Finally, the `constraints_are_periodic` variable may be used to enable or disable the free boundary conditions.

The core of the `LaplaceSolver` has been implemented based on the `deal.ii` tutorial. The developer interested to extend the code of this class (for example to enable computation on cluster) should refer to this useful resource [4].

The results are retrieved from a `LaplaceSolver` object calling the
`void get_solution(Solution<dim> &sol)` method with a properly allocated `Solution` object as parameter. The results are encapsulated in a `Solution` object. Thanks to this abstraction layer, it is possible to modify code in the class `LaplaceSolver` or in the class `Solution` without having to change code in other places in the program (as long as the interfaces of these classes are not changed). For example it may be useful if one decides not to use `deal.ii` anymore or if the data structure containing the results is changed.

The `Solution` class provides a method to access efficiently physical quantities at any location in the grid as well as methods to output graphs of the potential or the gradient of the potential. The physical quantities are accessed efficiently thanks to the `rtree` data structure already introduced in Section 3. The `rtree` implementation used in this class is provided by the famous `boost` C++ library [1]. This implementation also supports 3D search spaces.

The `Detector2D` class is an abstract class that models a detector represented by a two-dimensional geometry (a section of a detector). Implementation of this abstract class composes instances of the previously presented classes (`MyGeometryInfo`, `LaplaceSolver`, `BoundaryConditions` ,...).

Classes implementing the `Detector2D` abstract class must implement the following methods (much of them are already implemented in the `Detector2D` class and are therefore common to all types of detector):

- `void comp_potential()`: this method computes the potential at each point of the detector.
- `void comp_weight_potential()`: this method computes the weighting potential at each point of the detector.

- `MyGeometryInfo* get_geometry_info()`: returns a pointer to a `MyGeometryInfo` containing all useful informations about the geometry of the detector.
- `void get_solution(Solution<2> &sol)`: provides a `Solution<2>` object allowing to retrieve the potential and the electric field at any point of the grid. Must be called after one call to `void comp_potential()` with a properly instantiated `Solution<2>` object as parameter.
- `void get_solution_weight(Solution<2> &sol)`: provides a `Solution<2>` object allowing to retrieve the weighting potential and the weighting electric field at any point of the grid. Must be called after one call to `void comp_weight_potential()` with a properly instantiated `Solution<2>` object as parameter.
- `Hole get_hole()`: returns a `Hole` object having properties (mobility,...) corresponding to the type of the detector (helium, silicon).
- `Electron get_electron()`: returns an `Electron` object having properties (mobility,...) corresponding to the type of the detector (helium, silicon).
- `double get_hole_pairs_nbr_per_lgth()`: returns the number of ion-pairs per length generated by the particle pass in this type of detector (helium or silicon).
- `double get_strip_potential()`: return the potential of the potential sources in the detector.
- `double get_first_townsend_coefficient(Point<2> &pos, PhysicalValues<2> &values_at_pos)`: returns the first Townsend coefficient required to generate new ion-pairs due to the Townsend avalanche effect. For silicon detectors for which this effect does not apply, 0 is returned.
- `virtual std::string params_to_string()`: returns a string containing the values of the most important parameters of the detector.
- `void draw_vtk_graph_*`: this set of methods output some `vtk` files. These files contain a graphic representation of the potential and electric field. These files can be opened by the `Paraview` software.

The last important class is the class `ElectrodeCurrent`. This class is responsible of the computation of the current measured by the detector. Its constructor is presented at Listing 2.

```
ElectrodeCurrent(Detector2D *det, Line particle_trajectory,
                 unsigned refine_level)
```

Listing 2: Constructor of the `ElectrodeCurrent` class.

The first parameter `Detector2D *det` is a pointer to a detector of any kind (any geometry, gas, silicon), implementing the abstract class `Detector2D`. The second parameter is the particle trajectory. The last parameter `refine_level` controls the granularity of the current computation. A higher `refine_level` implies smaller time intervals (Δt) and a spread of the ion-pairs among more punctual charges along the particle trajectory.

The current computation starts once the method `compute_current` is called. The user can chose to impose a Δt himself. If he choses to do so, the same Δt is used throughout the entire computation.

Otherwise, the adaptive Δt strategy is used: the program computes himself an appropriate Δt at each iteration depending on the maximum charge velocity of the previous iteration.

C Comments on the academic activity

Throughout the realization of this work, we learned the basics of particle detectors physics. Furthermore, we learned to use the *deal.ii* library to solve partial differential equations and how to tackle some difficulties specific to the development of a numerical software.

The work achieved by each author, the number of days spent on this work and other statistics can be retrieved from the github repository of the project: `https://github.com/aschils/pdetect`. In total, 108 days has been spent on this project, a significant part of them being entire work days. The software is composed of 5209 lines of *C++* code and more than 438 commits have been pushed to the repository.

The most time-consuming task of this work was to learn the *deal.ii* library. It is a quite low level library with a lot of functionalities. A huge amount of time has been spent on technical details about the library and the programming language. The architecture of the software has been changed dozens of times in order to keep a clean architecture in agreement with the *deal.ii* abstractions.

Maybe it would be easier to learn the library if we had followed a course on finite element method beforehand. However, we do not think it would have an impact on the resulting software since we are using finite element method as a black box. Solving the Laplace equation being a very common problem it was easy to find examples solving this equation in the *deal.ii* tutorial.

The *C++* language has been selected because it is mastered by the two authors of this work. Moreover, it is the language instructed to physicists at our university allowing other students to work on the same project in the future. Retrospectively, maybe it would have been more judicious to develop this software in a higher level programming language such as *Python*. It would allow to develop the software faster. Besides the programming language choice, we think the problem has been approached properly.

The teamwork went well. We used the git distributed version control system to work properly together on the same source code. At the beginning of the project we developed the same pieces of software our separate ways in order to get used to the *deal.ii* library. Then, Simon took care of adaptive grid refinement, retrieval of errors on the potential from *deal.ii* and drawing of several kind of graphs (potential along a vertical line,...). Arnaud developed the generation of the grids for the different geometries, some geometry related code and the detector current computation. Broadly, each one has worked across the entire code to perform various modifications.

References

[1] Boost rtree data structure. http://www.boost.org/doc/libs/1_60_0/libs/geometry/doc/html/geometry/reference/spatial_indexes/boost__geometry__index__rtree.html.

[2] Comsol multiphysics - simulation tool for electrical, mechanical, fluid flow, and chemical applications. https://www.comsol.com/comsol-multiphysics.

[3] Condition number. https://en.wikipedia.org/wiki/Condition_number.

[4] The deal.ii tutorial. https://dealii.org/8.4.0/doxygen/deal.II/Tutorial.html.

[5] An example of the meshworker framework with an advection problem. https://dealii.org/8.4.0/doxygen/deal.II/step_12.html.

[6] Finite element method. https://en.wikipedia.org/wiki/Finite_element_method.

[7] Galerkin method. https://en.wikipedia.org/wiki/Galerkin_method.

[8] Garfield - simulation of gaseous detectors. http://garfield.web.cern.ch/garfield/.

[9] hp-fem. https://en.wikipedia.org/wiki/Hp-FEM.

[10] Implementation of a hybridizable discontinuous galkerin method for the convection-diffusion equation. https://dealii.org/8.4.0/doxygen/deal.II/step_51.html.

[11] Linear solver classes. https://dealii.org/8.4.0/doxygen/deal.II/group__Solvers.html.

[12] W. Bangerth, R. Hartmann, and G. Kanschat. Deal.ii - a general-purpose object-oriented finite element library. *ACM Trans. Math. Softw.*, 33(4), August 2007.

[13] W. Bangerth, T. Heister, L. Heltai, G. Kanschat, M. Kronbichler, M. Maier, and B. Turcksin. The deal.II library, version 8.3. *Archive of Numerical Software*, 4:1–11, 2016.

[14] Wolfgang Bangerth. Finite element methods in scientific computing. http://www.math.tamu.edu/~bangerth/videos/676/slides.34.pdf.

[15] Thomas Carraro and Sven Wetterauer. On the implementation of the extended finite element method (xfem) for interface problems. 2015.

[16] Francesca Cenna, N. Cartiglia, M. Friedl, B. Kolbinger, H.F.-W. Sadrozinski, A. Seiden, Andriy Zatserklyaniy, and Anton Zatserklyaniy. Weightfield2: A fast simulator for silicon and diamond solid state detector. *Nuclear Inst. and Methods in Physics Research, A*, 796(Complete):149–153, 2015.

[17] Eduardo Cortina Gil. Ionizing radiation measurement: detectors and nuclear electronics, chapter 4: Gas detectors.

[18] Haixin Liu and D. Jiao. A direct finite-element-based solver of significantly reduced complexity for solving large-scale electromagnetic problems. In *Microwave Symposium Digest, 2009. MTT '09. IEEE MTT-S International*, pages 177–180, June 2009.

[19] L. Rossi, P. Fischer, T. Rohe, and N. Wermes. *Pixel Detectors From Fundamentals to Applications*. Particle acceleration and detection. Springer, 2006.

[20] H. Spieler. *Semiconductor Detector Systems*. Series on Semiconductor Science and Technology. OUP Oxford, 2005.